International Journal of Bioprinting

RESEARCH ARTICLE

# Design and biomechanical analysis of patient-specific porous tantalum prostheses for knee joint revision surgery

**Shilong Mao[1†], Yang Liu[1†], Fuyou Wang[2], Peng He[3], Xianzhe Wu[3*], Xingshuang Ma[1*], Yanfeng Luo[1*]**

[1]College of Bioengineering, Chongqing University; Key Laboratory of Biorheological Science and Technology (Chongqing University), Ministry of Education, Chongqing, 400030, China

[2] Southwest Hospital of Army Medical University, Chongqing, 400038, China

[3]Chongqing Institute of Optics and Mechanics, Chongqing, 401122, China

(This article belongs to the *Special Issue: Additive Manufacturing of Functional Biomaterials*)

## Abstract

Artificial joint revision surgery, as an increasingly common surgery in orthopedics, often requires patient-specific prostheses to repair the bone defect. Porous tantalum is a good candidate due to its excellent abrasion and corrosion resistance and good osteointegration. Combination of 3D printing technology and numerical simulation is a promising strategy to design and prepare patient-specific porous prostheses. However, clinical design cases have rarely been reported, especially from the viewpoint of biomechanical matching with the patient's weight and motion and specific bone tissue. This work reports a clinical case on the design and mechanical analysis of 3D-printed porous tantalum prostheses for the knee revision of an 84-year-old male patient. Particularly, standard cylinders of 3D-printed porous tantalum with different pore size and wire diameters were first fabricated and their compressive mechanical properties were measured for following numerical simulation. Subsequently, patient-specific finite element models for the knee prosthesis and the tibia were constructed from the patient's computed tomography data. The maximum von Mises stress and displacement of the prostheses and tibia and the maximum compressive strain of the tibia were numerically simulated under two loading conditions by using finite element analysis software ABAQUS. Finally, by comparing the simulated data to the biomechanical requirements for the prosthesis and the tibia, a patient-specific porous tantalum knee joint prosthesis with a pore diameter of 600 μm and a wire diameter of 900 μm was determined. The Young's modulus (5719.32 ± 100.61 MPa) and yield strength (172.71 ± 1.67 MPa) of the prosthesis can produce both sufficient mechanical support and biomechanical stimulation to the tibia. This work provides a useful guidance for designing and evaluating a patient-specific porous tantalum prosthesis.

***Keywords:*** Porous tantalum; Finite element analysis; Artificial joint revision surgery; Biomechanics

†These authors contributed equally to this work.

***Corresponding authors:**
Xianzhe Wu
(cqrptad@126.com)

Xingshuang Ma
(maxs@cqu.edu.cn)

Yanfeng Luo
(yfluo@cqu.edu.cn)

**Citation:** Mao S, Liu Y, Wang F, *et al*., 2023, Design and biomechanical analysis of patient-specific porous tantalum prostheses for knee joint revision surgery. *Int J Bioprint*.
https://doi.org/10.18063/ijb.735

**Received:** November 24, 2022
**Accepted:** January 30, 2023
**Published Online:** April 20, 2023

## 1. Introduction

Artificial knee arthroplasty is one of the most common and successful orthopedic surgeries for the treatment of end-stage knee disease[1]. However, after the joint replacement, a series of complications such as infection, bone resorption, or aseptic loosening may require joint revision surgery. Among various materials for joint revision surgery, porous tantalum has attracted extensive attention because of its clinically validated excellent abrasion, corrosion resistance, and osteointegration[2-5]. More importantly, it has been noticed from joint revision surgery that the geometrical shape of bone defects and the mechanical properties of surrounding bone tissue vary with patients and bone defect sites. Consequently, the commercialized standard modular blocks cannot match the bone defect region geometrically and biomechanically. Development of patient-specific porous tantalum prostheses with matching shape and biomechanics may help to increase the success rate of joint revision surgery.

Extensive tracks and clinical follow-up observations have proven that porous tantalum as various prostheses can induce strong osteointegration and produce satisfactory repair outcomes[6-11]. The earliest technology employed to fabricate porous tantalum is chemical vapor deposition[12]. The representative manufacturer is Zimmer. Tantalum has a high melting point of ~2996°C[13]. With the development of 3D printing technologies, some technologies capable of providing a temperature high enough to melt tantalum, such as electron-beam-melting-based and laser-melting-based technologies, are being employed to fabricate porous tantalum[14-16]. The fabricated porous tantalum prostheses geometrically match well with the bone defect and result in effective osteointegration and treatment[16]. In addition to geometrical matching, ideal patient-specific porous tantalum prostheses should have appropriate mechanical properties to guarantee the mechanical safety of both the prostheses and the bone tissue[17-20]. Therefore, regulating and measuring the mechanical properties of tantalum prostheses seem critically important.

Pore size and wire diameter are two critical parameters in 3D printing to regulate the mechanical properties of scaffolds. However, it is difficult to carry out *in vivo* mechanical tests on the implanted prostheses or the bone tissue. Therefore, numerical simulation of the *in vivo* biomechanical responses by using finite element analysis (FEA) becomes a more effective approach[21-23]. FEA can provide the mechanical responses of bone tissue[24-26] and prostheses[27-30] under various mechanical environments, which in turn is valuable to guide the design and fabrication of prostheses. Despite the wide applications of FEA, few studies were reported on its application in the clinical design of patient-specific 3D-printed porous tantalum prostheses, especially in the evaluation of the designed prostheses from the viewpoint of bone biomechanics.

This paper reports a clinical case on the application of FEA in designing patient-specific tantalum prostheses with an appropriate pore size and wire diameter for knee joint revision. Particularly, standard porous tantalum cylinders with various pore sizes and wire diameters were first fabricated by using a selective laser printing technology and their compressive mechanical properties were measured. Subsequently, FEA models on the patient-specific tibia and prostheses were developed from the patient's computed tomography (CT) data. By using the models, the maximum von Mises stress and displacement for porous tantalum prostheses and tibia and the maximum strain for the tibia were numerically simulated. Finally, according to the biomechanical requirements on both the prostheses and the tibia, the tantalum prostheses with appropriate pore size and wire diameter were determined. This work provides a valuable reference for the clinical design of porous tantalum prostheses for joint revision surgery.

## 2. Materials and methods

### 2.1 Mechanical test

Seven kinds of standard cylinder porous tantalum samples (diameter 15 mm, height 20 mm) with a pore shape of dodecahedron were manufactured using a selective laser melting (SLM; FARSOON Technology, China) system by Zhuzhou Printing Additive Manufacturing Co. Ltd in Hunan Province, China. The fabrication was performed in argon atmosphere with a laser power of 250 W, a laser scanning speed of 150 mm/s, and an energy density of 241.5 J/mm$^3$. Different pore size (900–1500 μm) and wire diameter (300–600 μm) were selected. To simplify the description, the sample with a wire diameter of $m$ and a pore size of $n$ was recorded as $m/n$. The specific pore and wire diameter information is shown in Table 1.

The uniaxial compression mechanical tests were carried out by using AG-X50kND electronic universal material testing machine from SHIMADZU, Japan. All the test samples were compressed at a loading rate of 1 mm/min until 50% strain occurred. The diameter ($d$) and height ($h$) of the sample were measured with a caliper before experiment. The cross-sectional area of the sample ($A$) was calculated using $A = \pi \times (d/2)^2$. According to the obtained stress–strain curves, the Young's modulus and yield strength were calculated. At least three specimens were tested for each sample.

### 2.2. Construction of the tibia and prosthesis models

The patient was an 84-year-old male with severe osteoarthritis in his left knee. After 16 years of left knee

**Table 1. Pore structure information and compressive mechanical properties of standard porous tantalum cylinders**

| Sample | Wire diameter (μm) | Pore diameter (μm) | Porosities (%) | Mechanical properties (MPa) | |
|---|---|---|---|---|---|
| | | | | Young's modulus | Yield strength |
| 300/1200 | 300 | 1200 | 93.71 | 1302.83 ± 76.96 | 23.25 ± 0.06 |
| 450/900 | 450 | 900 | 82.37 | 4998.09 ± 69.74 | 106.36 ± 0.17 |
| 450/1200 | 450 | 1200 | 88.11 | 2968.83 ± 31.76 | 76.19 ± 0.65 |
| 450/1500 | 450 | 1500 | 91.60 | 2907.64 ± 14.04 | 49.14 ± 0.64 |
| 600/900 | 600 | 900 | 76.46 | 5719.32 ± 100.61 | 172.71 ± 1.67 |
| 600/1200 | 600 | 1200 | 83.32 | 4660.56 ± 187.07 | 109.19 ± 1.40 |
| 600/1500 | 600 | 1500 | 87.24 | 3743.04 ± 36.77 | 78.45 ± 1.01 |

arthroplasty, severe pain forced him to receive a revision surgery. The CT imaging data of the patient were collected and provided by Southwest Hospital of Army Medical University. Specifically, the two-dimensional image data of the full length of the patient's lower extremities, i.e., from the pelvic position to below the ankle position, were collected using a spiral CT machine (Siemens Inc, Germany) with a scanning angle of 360° at the Southwest Hospital of Army Medical University. The scan layer thickness and kilovoltage peak (kVp) were set as 1.5 mm and 140 kV, respectively. Medical image processing software Mimics 20.0 (Materialise NV, Belgium) and Geomagic Studio 2013 (Geomagic Inc, USA) were utilized to reconstruct the patient's 3D tibia bone model. Based on the constructed tibia bone model, a patient-specific prosthesis geometrically matching the bone defect site in the tibia was designed by using CAD design software NX 12.0 (Siemens PLM, USA).

### 2.3. Finite element simulation

The finite element models of the prosthesis and tibia were constructed and simulated using finite element simulation software ABAQUS 6.12 (SIMULIA, USA). Ten-node secondary tetrahedral element (C3D10) was used in this study. Before presenting the results, a mesh study was conducted to solve the mesh dependence problem. Four mesh sizes of the tibia were employed to compare the stress situation. The mesh size resulting in minimum computational time was regarded as appropriate.

#### *2.3.1. Material properties*

The material property of the porous tantalum prosthesis was defined as an isotropic homogeneous material. The Young's modulus of the prosthesis was assigned according to the equivalent Young's modulus of tantalum samples obtained from uniaxial tests in section 2.1. Poisson's ratio was 0.3. The material property of the patient's tibia, according to previous reports[31,32], was assigned as cortical bone with an elastic modulus of 20,000 MPa and Poisson's ratio of 0.3.

#### *2.3.2. Boundary conditions*

A general analysis of static mechanics with binding contact between the tantalum prosthesis and the tibia was used. In this case, the lower end of the tibia was fixed in all direction, while the load was uniformly distributed over the tibia plateau at the upper end of the prosthesis. Based on the patient's weight (71 kg), a uniform force of F1 = 350 N was applied to the upper end of the prosthesis to simulate the normal standing posture on two legs, and a uniform force of F2 = 700 N was applied to simulate the patient's standing posture on single leg and climbing stairs postures. The boundary conditions for the FE model considering both the load and the restriction of movement are illustrated in Figure 1d.

#### *2.3.3. Maximum strain calculation*

The maximum strain ($\varepsilon$) of the tibia was employed to indicate the biomechanical response of the tibia. The $\varepsilon$ was calculated using $\varepsilon = \sigma/E$, where $\sigma$ is the von Mises stress of bone tissue adjacent to the prosthesis and $E$ is the Young's modulus of bone tissue.

## 3. Results

### 3.1. Mechanical test

Figure 2 shows the fabricated standard cylinders of porous tantalum and their typical compression stress–strain curves. The initial nonlinear phase of the stress–strain curve should be a result of some small uneven struts yielding locally[33-35]. The Young's modulus was represented by the slope of the linear range of the curves. The yield strength was defined as the stress at 0.2% offset strain since the yield points were not clear[36]. The Young's modulus and yield strength of the samples are summarized in Table 1.

The pore size and wire diameter were observed to significantly influence the mechanical properties of the 3D-printed porous tantalum. Specifically, for a predetermined pore size, both the Young's modulus and yield strength increased with the increasing wire diameter. On the other hand, for a predetermined wire diameter, both the

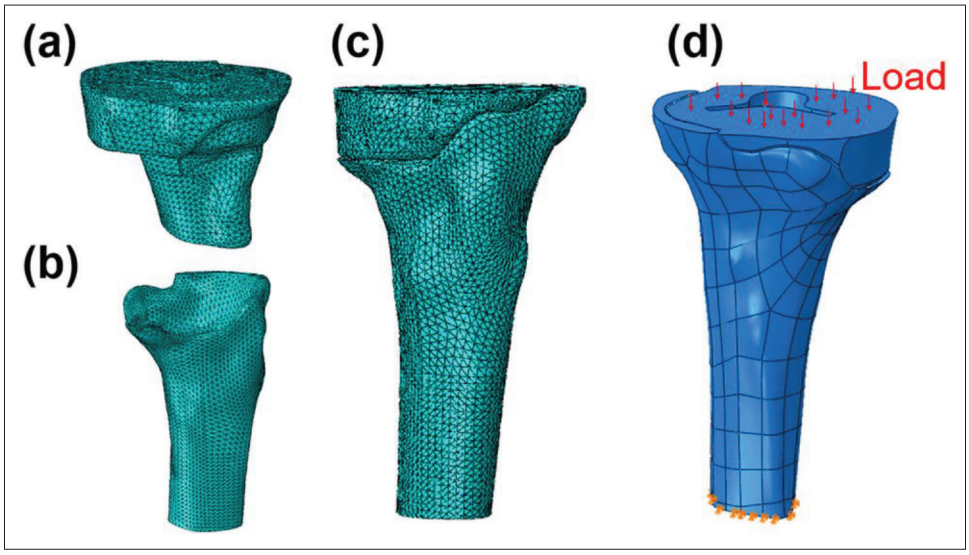


**Figure 1**. Illustration of the finite element models for (a) the prosthesis, (b) the tibia, (c) the assembly, and (d) the boundary and loading conditions.

Young's modulus and the yield strength decreased with the increasing pore size. The sample 300/1200 demonstrated the minimum Young's modulus (1302.83 ± 76.96 MPa) and yield strength (23.25 ± 0.06 MPa), whereas the sample 600/900 saw the maximum Young's modulus of 5719.32 ± 100.61MPa and yield strength of 172.71 ± 1.67 MPa.

### 3.2. Construction of the tibia and prosthesis models

Figure 3a shows the constructed tibia model from the CT data of the patient. An obvious bone defect was observed on the tibia adjacent to the artificial knee joint (arrow indicated). In order for implantation of a new total knee arthroplasty (TKA), a patient-specific prosthesis (Figure 3b) to the tibia defect (Figure 3c) was designed, and its *in vivo* position in the tibia (Figure 3d) was simulated. The obtained models were used for the following FEA simulation in this work.

### 3.3. Finite element simulation

Four mesh sizes of the tibia were employed to compare the stress situation. The number of the total meshes in each model was Grid1 = 79,671, Grid2 = 81,422, Grid3 = 105,145, and Grid4 = 128,701. Figure 4 shows the mesh dependency based on the maximum von Mises stress of the tibia. The accessible error between the Grid3 and the Grid4 model was 7.9%. Since Grid3 resulted in a less computational time than Grid4, Grid3 was chosen as the source mesh. The final number of meshes was 105,145, including 58,858 meshes for prosthesis (Figure 1a) and 46,287 meshes for patient's tibia (Figure 1b).

Since the constructed prosthesis model geometrically matched well with the tibia (Figures 1c and 3d), a general analysis of static mechanics with binding contact was used for FEA simulation. According to the boundary conditions shown in Figure 1d, the von Mises stress and displacement of the tantalum prosthesis and the tibia at a standing posture on single leg and on two legs were numerically simulated. The maximum von Mises stress occurred at the contact region between the prosthesis and the tibia (Figures 5a and 6a), whereas the maximum displacement appeared on the upper surface of the prosthesis (Figures 5b and 6b).

For ease of comparison, the maximum von Mises stress and maximum displacement of various prostheses and the corresponding values for the tibia were collected and shown in Table 2 for single-leg standing posture and in Table 3 for two-leg standing posture. The maximum strain of the tibia adjacent to the prosthesis was further simulated. When standing on single leg (Table 2), the maximum von Mises stress varied from 24.56 MPa (300/1200) to 26.87 MPa (600/900) for the prostheses and from 53.65 MPa (600/900) to 69.64 MPa (300/1200) for the tibia. All of the prostheses and tibia demonstrated small displacement of less than 0.15 mm. It is worth noting that the maximum strain of the tibia varied from 2682.5 με (600/900) to 3482.5 με (300/1200), and only those tibias adjacent to the prostheses 450/900, 600/1200, 600/1500, and 600/900 demonstrated a maximum strain in the range of 400–3000 με. Regarding the standing posture with two legs (Table 3), the maximum von Mises stress values of the prostheses and tibia were all smaller than their corresponding values for single-leg standing posture. The prostheses saw the maximum von Mises stress from 12.28 MPa (prosthesis 300/1200) to 13.44 MPa (prosthesis 600/900) and the tibia saw the maximum von Mises stress from 26.82 MPa (prosthesis 600/900) to 34.82 MPa (prosthesis 300/1200). The maximum node displacements

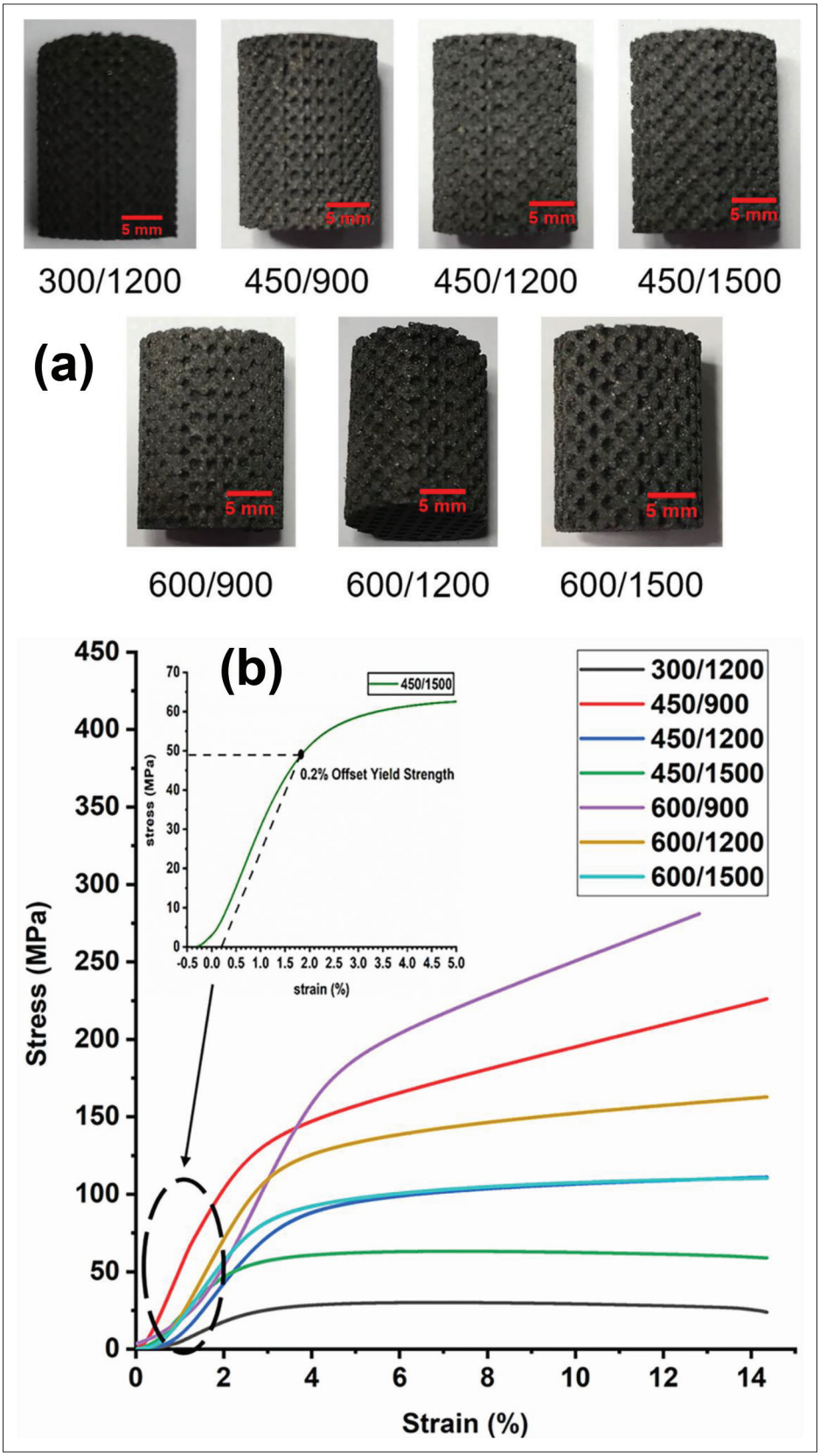


**Figure 2**. The standard porous tantalum cylinders (*m*/*n*) with various wire diameters (*m*) and pore sizes (*n*) (a) and their compressive stress–strain curves (b).

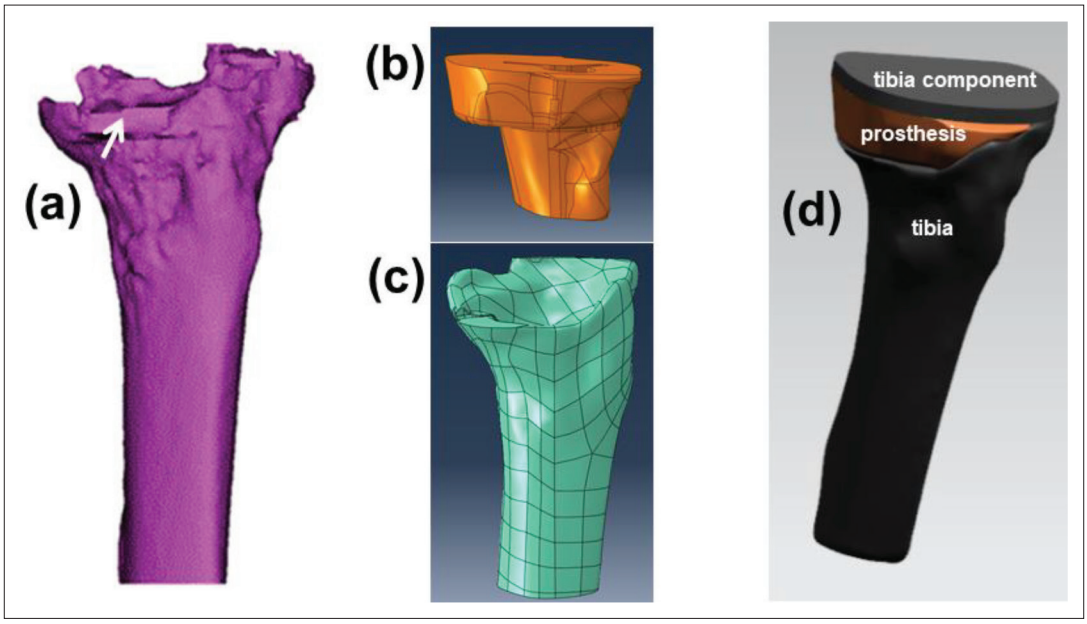


**Figure 3**. 3D models for the constructed tibia and prosthesis. (a) The original tibia constructed from the CT data; the arrow indicates the defect site. (b) The designed prosthesis. (c) The polished tibia. (d) The assembly.

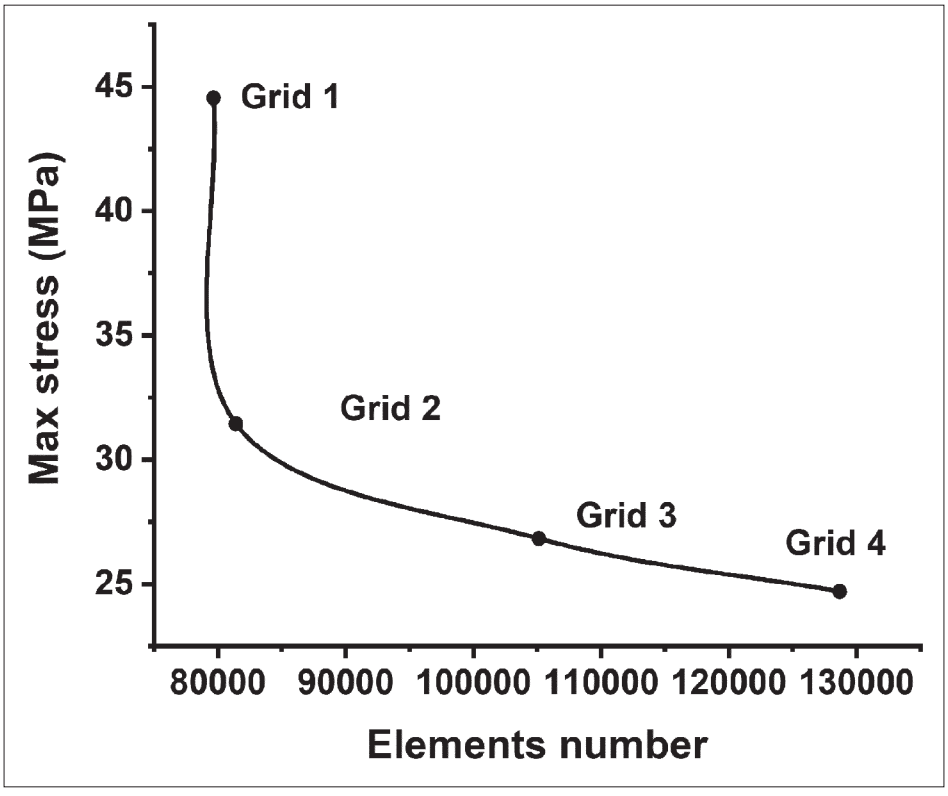


**Figure 4**. Mesh dependency of the maximum von Mises stress of the tibia.

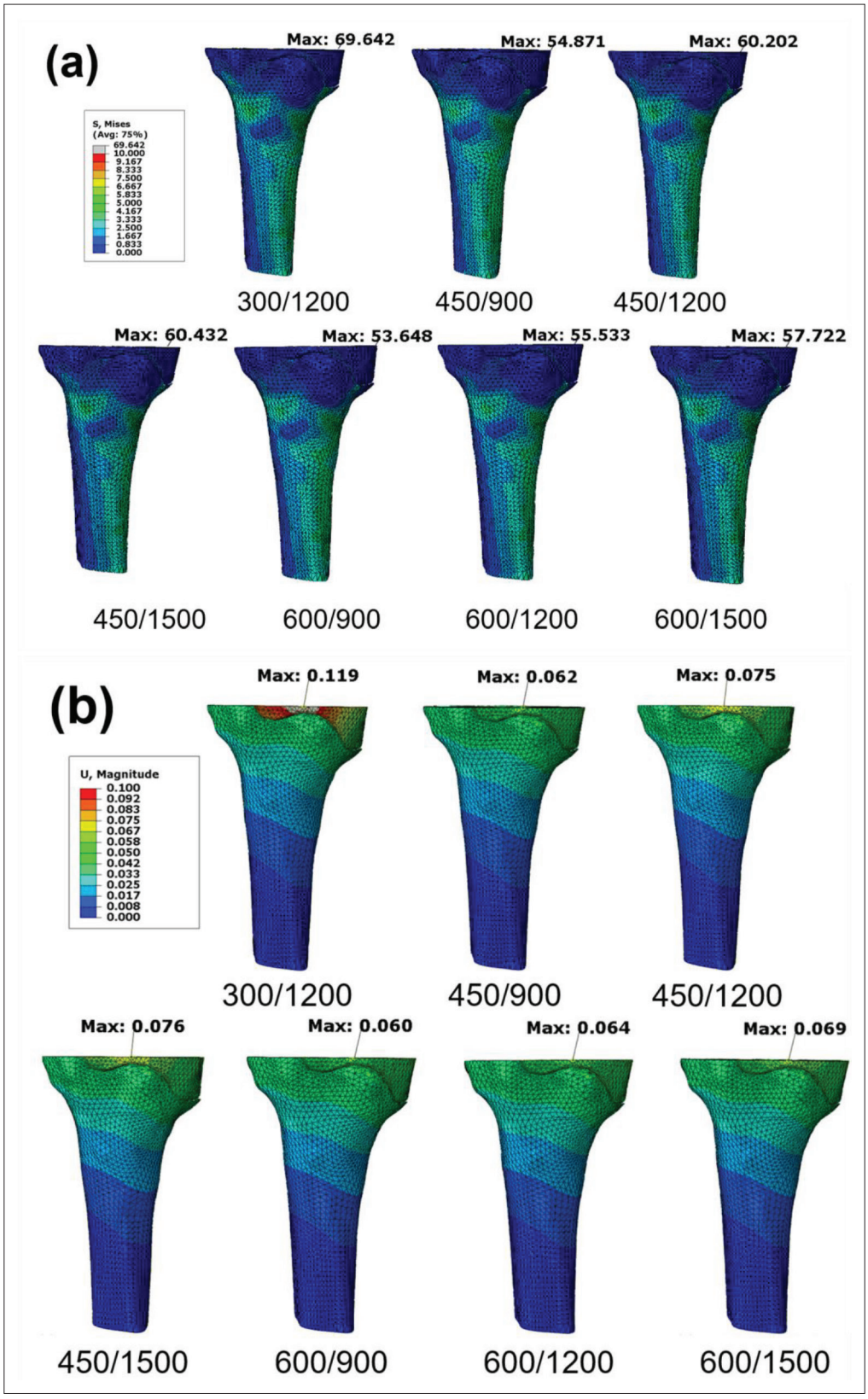


**Figure 5**. von Mises stress distribution (a) and node displacement distribution (b) of the prosthesis and tibia at a single-leg standing posture.

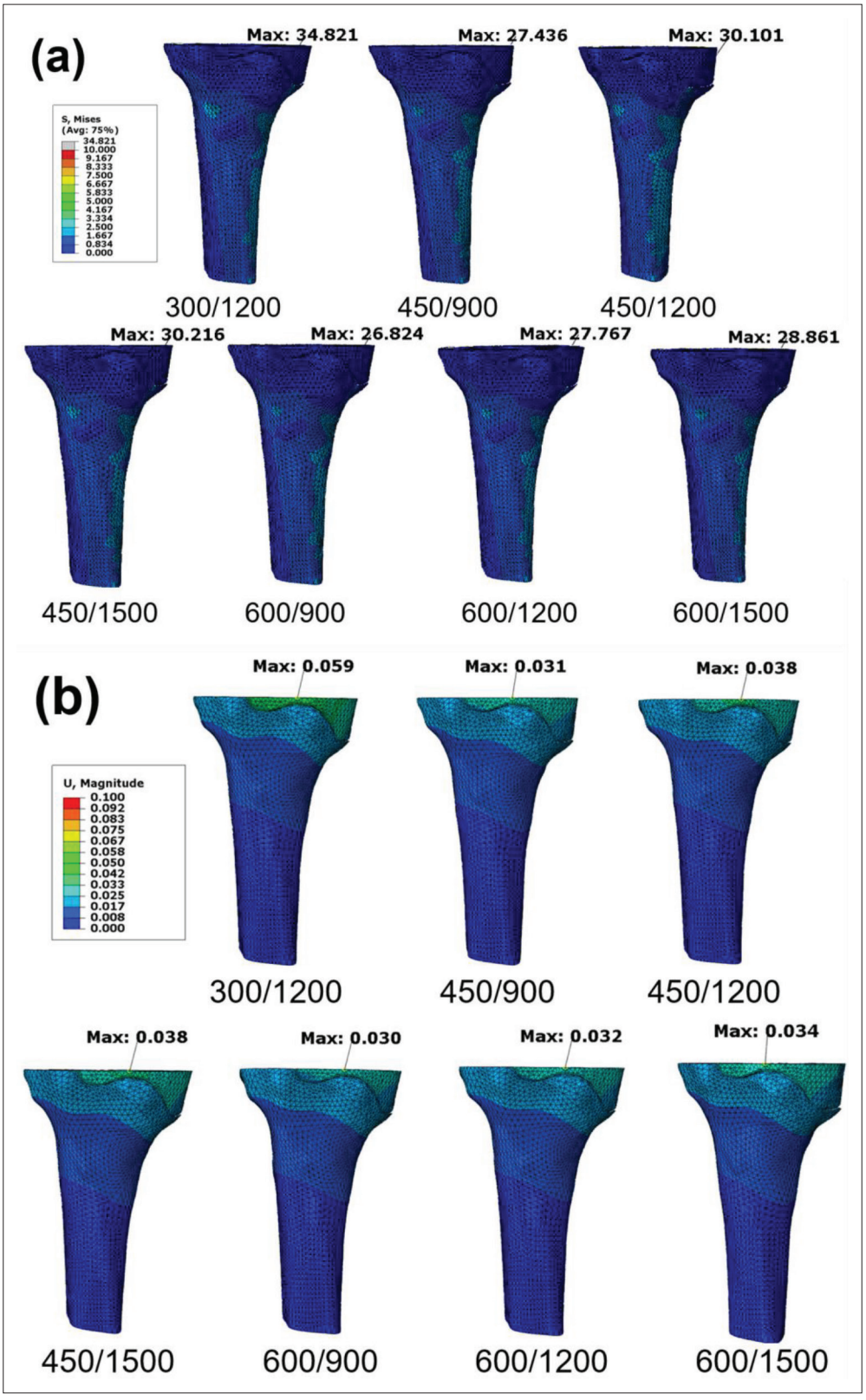


**Figure 6**. von Mises stress distribution (a) and node displacement distribution (b) of the prosthesis and tibia at a two-leg standing posture.

**Table 2. Maximum von Mises stress and node displacement of the prostheses and tibia at a single-leg standing posture**

| Sample | Maximum von Mises stress (MPa) | | Maximum displacement (mm) | | Maximum strain of tibia (με) |
|---|---|---|---|---|---|
| | Prostheses | Tibia | Prostheses | Tibia | |
| 300/1200 | 24.56 | 69.64 | 0.11890 | 0.04871 | 3482.0 |
| 450/900 | 26.67 | 54.87 | 0.06250 | 0.04523 | 2743.5 |
| 450/1200 | 25.85 | 60.20 | 0.07526 | 0.04651 | 3010.0 |
| 450/1500 | 25.82 | 60.43 | 0.07594 | 0.04656 | 3021.5 |
| 600/900 | 26.87 | 53.65 | 0.06025 | 0.04493 | 2682.5 |
| 600/1200 | 26.57 | 55.53 | 0.06381 | 0.04539 | 2776.5 |
| 600/1500 | 26.22 | 57.72 | 0.06865 | 0.04592 | 2886.0 |

**Table 3. Maximum von Mises stress and node displacement of the prostheses and tibia at a two-leg standing posture**

| Sample | Maximum von Mises stress (MPa) | | Maximum displacement (mm) | | Maximum strain of tibia (με) |
|---|---|---|---|---|---|
| | Prostheses | Tibia | Prostheses | Tibia | |
| 300/1200 | 12.28 | 34.82 | 0.05946 | 0.02435 | 1741.0 |
| 450/900 | 13.34 | 27.44 | 0.03125 | 0.02262 | 1372.0 |
| 450/1200 | 12.93 | 30.10 | 0.03763 | 0.02326 | 1505.0 |
| 450/1500 | 12.91 | 30.22 | 0.03797 | 0.02328 | 1511.0 |
| 600/900 | 13.44 | 26.82 | 0.03012 | 0.02247 | 1341.0 |
| 600/1200 | 13.28 | 27.77 | 0.03190 | 0.02270 | 1388.5 |
| 600/1500 | 13.11 | 28.86 | 0.03432 | 0.02296 | 1443.0 |

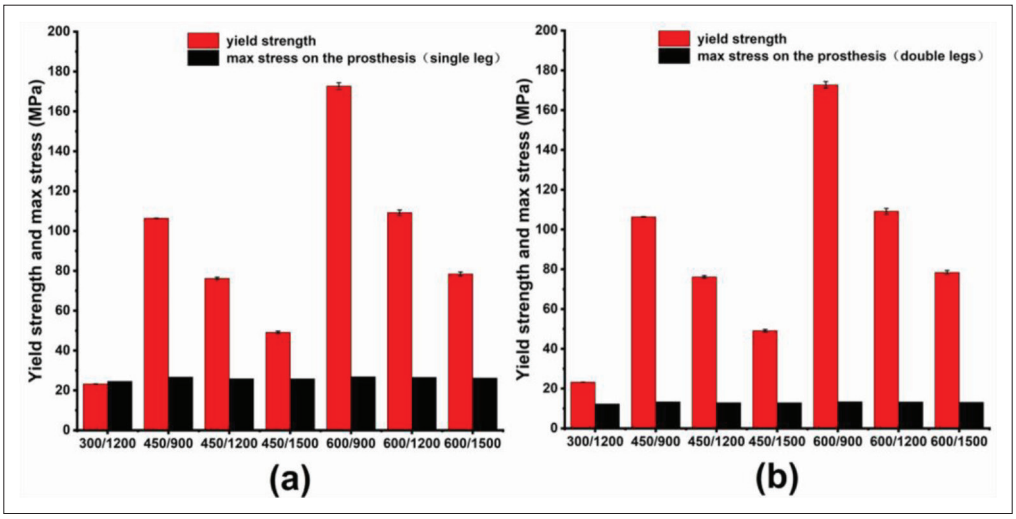


**Figure 7**. Comparison of the yield strength and the maximum von Mises stress of the prostheses at a single-leg (a) and two-leg (b) standing posture.

of all the prostheses and tibia were less than 0.06 mm. Comparison of the maximum von Mises stress indicated that the tibia always had a higher maximum von Mises stress than the corresponding prosthesis (Tables 2 and 3).

To indicate the potential of the porous tantalum prostheses to resist the mechanical loading from the patient weight and standing postures, the yield strength and the maximum von Mises stress of the prostheses are listed and compared in Figure 7. It was noted that, with single-leg standing posture, the maximum von Mises stress of the prosthesis 300/1200 exceeded its yield strength, suggesting that the prosthesis 300/1200 is too weak to be eligible for the revision surgery.

## 4. Discussion

It is well known that artificial knee arthroplasty is an effective orthopedic surgery for the treatment of the end-stage knee

disease. Porous tantalum has been widely used in primary and revision joint replacement surgery for more than 20 years, yet the clinical design of patient-specific porous tantalum prostheses has rarely been reported. In this work, we designed a patient-specific porous tantalum prosthesis from the viewpoint of biomechanics with the help of FEA. The designed prosthesis geometrically and biomechanically matches well with the defected tibia of the patient.

The mechanical properties of porous tantalum are indispensable parameters for FEA-based numerical simulation. Pore shape, pore size, and wire diameter are the main factors influencing the mechanical properties of a 3D-printed scaffold. In this work, the pore shape was set as dodecahedron, a pore shape similar to that in cancellous bone[37,38]. Theoretically, the pore size and wire diameter can be set as any value. However, the limit of printing precision generally determines the minimum wire diameter. Accordingly, in this work, the wire diameter from 300 to 600 μm and the pore size from 600 to 1500 μm were selected (Table 1), and SLM was employed to print the standard porous tantalum samples (Figure 1a). The Young's modulus and yield strength (Table 1) were collected to provide mechanical parameters for FEA numerical simulation and biomechanical evaluation.

To realize the patient-specific design of prosthesis, the 3D models of both the prosthesis and the tibia were constructed from the CT imaging data of the patient (Figure 2a), and the shape of the prosthesis was designed to match well with the bone defect (Figure 2b and 2c). It is known that the bone tissue is a stress-sensitive tissue and the perceived stress by bone tissue directly affects the growth of bone tissue[39-43]. Accordingly, in addition to the geometrical matching, the biomechanical matching of the prosthesis was proposed as well in this work.

Imaginably, after the prosthesis is implanted into the bone defect site, the mechanical loading, originating from the patient's weight and motion, is applied to the prosthesis and then transferred to the tibia. Therefore, the magnitude of the perceived stress by the tibia is closely related to the mechanical properties of the prosthesis. Ideally, at least three basic requirements for the mechanical properties of the prosthesis should be satisfied. First, the compressive strength should be high enough to withstand the mechanical load. That is, the prosthesis should have mechanical safety. This can be satisfied should the yield strength of the prosthesis be higher than the exerted compressive stress. Second, the Young's modulus of the prosthesis should be appropriate to allow the transmission of sufficient mechanical load to the tibia and induce enough strain to stimulate tibia growth, by which stress shielding is avoided. This can be defined as biomechanical effectiveness of the prosthesis. Frost[19] and Cowin[20] found that human physiological strain (400–3000 με) is beneficial to bone tissue's growth. Lower strain (<50–100 με) leads to bone resorption and higher strain (>3000 με) may damage bone tissue. Therefore, in this work, a Young's modulus promising a tibia strain of 400–3000 με can be regarded to satisfy the biomechanical effectiveness. Third, the transmitted mechanical load from the prosthesis to the tibia cannot be too high and damage the tibia, which means that the prosthesis should promise the bone mechanical safety. Some studies have indicated that the yield strength of cortical bone tissue in healthy adults is close to 60 MPa; when the perceived stress exceeds 60 MPa (or strain exceeds ~3000 με), the bone tissue is liable to be damaged[20]. Therefore, when the perceived stress is less than 60 MPa, the prosthesis is mechanically safe to the bone. By comparing the simulated maximum von Mises stress and displacement and the maximum strain data with these three requirements, the biomechanical matching of the prosthesis can be evaluated and the appropriate wire diameter and pore size of prostheses can be determined.

(i) First, according to the requirement for prosthesis mechanical safety, the prosthesis with a wire diameter of 300 and a pore sized of 1200 (from samples 300/1200) should be excluded since its yield strength is lower than the maximum von Mises stress at single-leg standing posture and may lead to destruction of the prosthesis after the prosthesis is implanted (Figure 7).

(ii) Although all the maximum von Mises stresses of the tibia were obviously lower than 60 MPa at a two-leg standing posture, those prostheses from 450/1200 and 450/1500 demonstrated a maximum von Mises stress of >60 MPa at a single-leg standing posture. This means that, when these two prostheses are implanted, the tibia at a single-leg standing posture may be broken. Therefore, the prostheses from 450/1200 and 450/1500 cannot be used.

(iii) Regarding the rest prostheses from 450/900, 600/1200, 600/1500, and 600/900, the tibia strains produced by the transferred mechanical load from body weight and motion were all within 400–3000 με both at a single-leg standing posture and at a two-leg standing posture, satisfying the second requirement for bone biomechanical effectiveness.

In brief, the mechanical tests and numerical simulation indicate that the prostheses from 450/900, 600/1200, 600/1500, and 600/900 satisfy all the three requirements mentioned above and thus are suitable implants for the knee joint revision injury of the patient. The prosthesis from 600/900 was finally selected for clinical implantation

in 2017. Follow-up observations of about 5 years indicate that the designed and fabricated prosthesis integrates well with the surrounding bone tissue and the patient can take normal movements without any discomfort (data not shown), supporting our numerical simulation results. Our attempts by combining patient-specific design and numerical simulation of the 3D-printed prostheses provide a valuable paradigm for prostheses design and may help to improve the success rate of implants. However, it should be noted that, bone tissues are anisotropic and their mechanical properties are patient- and site-specific. Future work should take bone tissues as anisotropic rather than isotropic materials. In addition, a quantitative relationship between the patient's CT data and the bone mineral density and bone mechanical properties should be established, by which the patient- and site-specific bone remodeling process followed by implantation of the prostheses could be applied for FEA and biomechanical matching evaluation.

## 5. Conclusion

In this work, we successfully constructed FEA models for the tibia and the patient-specific prosthesis based on the patient's CT data. By using the models, together with the mechanical properties of 3D-printed porous tantalum and the patient's weight and postures, the maximum von Mises stress and displacement and compressive strain were simulated. Finally, by comparing the simulated data with the biomechanical requirements for the prosthesis, the porous tantalum prostheses with sufficient mechanical support to knee joint and matchable biomechanical stimulation to tibia were successfully determined. This work provides a valuable paradigm for designing and evaluating porous tantalum prostheses and may help to improve the success rate of implants.

## Acknowledgments

None.

## Funding

This study was funded by National Key Research and Development Plan of China (2016YFB1101401) and National Natural Science Foundation of China (No. 32271362).

## Conflict of interest

The authors declare no conflict of interest.

## Author contributions

*Conceptualization:* Xianzhe Wu, Xingshuang Ma, Yanfeng Luo
*Investigation:* Shilong Mao, Yang Liu
*Methodology:* Shilong Mao, Yang Liu, Fuyou Wang, Peng He
*Supervision:* Xianzhe Wu, Xingshuang Ma, Yanfeng Luo
*Writing – original draft:* Shilong Mao, Yang Liu
*Writing – review & editing:* Shilong Mao, Xingshuang Ma, Yanfeng Luo

All authors read and approved the manuscript for publication.

## Ethics approval and consent to participate

Research ethics approval has been obtained from the ethics committee of the Southwest Hospital of Army Medical University, China for this study (2016-J-001), and informed consent has been obtained from the patient for participating in this study.

## Consent for publication

The patient has consented to publish his relevant data in this work.

## Availability of data

All data used in this work are presented in the paper.

## References

1. Woiczinski M, Steinbrück A, Weber P, *et al.*, 2015, Development and validation of a weight-bearing finite element model for total knee replacement. *Comput Methods Biomech Biomed Eng*, 19(10):1033–1045.

   https://doi.org/10.1080/10255842.2015.1089534

2. Grelsamer RP, 2007, Applications of porous tantalum in total hip arthroplasty. *J Am Acad Orthop Surg*, 14(12):646–655.

   https://doi.org/10.1016/j.jse.2005.09.001

3. Matsuno H, Yokoyama A, Watari F, *et al.*, 2001, Biocompatibility and osteogenesis of refractory metal implants, titanium, hafnium, niobium, tantalum and rhenium. *Biomaterials*, 22(11):1253–1262.

   https://doi.org/10.1016/S0142-9612(00)00275-1

4. Zou X, Li H, Bünger M, *et al.*, 2004, Bone ingrowth characteristics of porous tantalum and carbon fiber interbody devices: An experimental study in pigs. *Spine J*, 4(1):99–105.

   https://doi.org/10.1016/S1529-9430(03)00407-8

5. Bobyn JD, Stackpool GJ, Hacking SA, *et al.*, 1999, Characteristics of bone ingrowth and interface mechanics of a new porous tantalum biomaterial. *J Bone Joint Surg Br*, 81(5):907–914.

   https://doi.org/10.1302/0301-620X.81B5.9283

6. Rossi SMP, Perticarini L, Ghiara M, *et al.*, 2022, High survival rate at mid-term follow up of porous tantalum

cones for bone defects in revision total knee replacement: A 3–11 years follow up report. *Knee*, 35(2022):175–182.

https://doi.org/10.1016/j.knee.2022.03.007

7. Huang G, Pan S, Qiu J, 2021, The clinical application of porous tantalum and its new development for bone tissue engineering. *Materials*, 14(10):2647.

https://doi.org/10.3390/ma14102647

8. Kamath AF, Gee AO, Nelson CL, *et al.*, 2012, Porous tantalum patellar components in revision total knee arthroplasty minimum 5-year follow-up. *J Arthroplast*, 27(1):82–87.

https://doi.org/10.1016/j.arth.2011.04.024

9. Kamath AF, Lee GC, Sheth NP, *et al.*, 2011, Prospective results of uncemented tantalum monoblock tibia in total knee arthroplasty: Minimum 5-year follow-up in patients younger than 55 years. *J Arthroplast*, 26(8):1390–1395.

https://doi.org/10.1016/j.arth.2011.06.030

10. Howard JL, Kudera J, Lewallen DG, *et al.*, 2011, Early results of the use of tantalum femoral cones for revision total knee arthroplasty. *J Bone Joint Surg Am*, 93(5):478–484.

https://doi.org/10.2106/JBJS.I.01322

11. Unger AS, Duggan JP, 2011, Midterm results of a porous tantalum monoblock tibia component clinical and radiographic results of 108 knees. *J Arthroplast*, 26(6):855–860.

https://doi.org/10.1016/j.arth.2010.08.017

12. Kaplan RB, 1994, Open cell tantalum structures for cancellous bone implants and cell and tissue receptors. *EP*, EP0560279 B1.

13. Thijs L, Sistiaga MM, Wauthle R, *et al.*, 2013, Strong morphological and crystallographic texture and resulting yield strength anisotropy in selective laser melted tantalum. *Acta Biomater*, 61(12):4657–4668.

https://doi.org/10.1016/j.actamat.2013.04.036

14. Song C, Deng Z, Zou Z, *et al.*, 2022, Pure tantalum manufactured by laser powder bed fusion: Influence of scanning speed on the evolution of microstructure and mechanical properties. *Int J Refract Metals Hard Mater*, 107(2022):105882.

https://doi.org/10.1016/j.ijrmhm.2022.105882

15. Gao H, Jin X, Yang J, *et al.*, 2021, Porous structure and compressive failure mechanism of additively manufactured cubic-lattice tantalum scaffolds. *Mater Today Adv*, 12(2021):100183.

https://doi.org/10.1016/j.mtadv.2021.100183

16. Tang HP, Yang K, Jia L, *et al.*, 2020, Tantalum bone implants printed by selective electron beam manufacturing (SEBM) and their clinical applications. *J Miner Metals Mater Soc*, 72(3):1016–1021.

https://doi.org/10.1007/s11837-020-04016-8

17. Risse L, Woodcock S, Brüggemann J, *et al.*, 2022, Stiffness optimization and reliable design of a hip implant by using the potential of additive manufacturing processes. *BioMed Eng OnLine*, 21(1):23.

https://doi.org/10.1186/s12938-022-00990-z

18. Kharmanda G, Gowid S, Mahdi E, *et al.*, 2020, Efficient system reliability-based design optimization study for replaced hip prosthesis using new optimized anisotropic bone formulations. *Materials*, 13(2):362.

https://doi.org/10.3390/ma13020362

19. Frost HM, 2004, A 2003 update of bone physiology and Wolff's law for clinicians. *Angle Orthod*, 74(1):3–15.

https://doi.org/10.1043/0003-3219(2004)0742.0.CO;2

20. Cowin SC, 2002, Mechanosensation and fluid transport in living bone. *J Musculoskelet Neuronal Interact*, 2(3):256–260.

21. Zupancic Cepic L, Frank M, Reisinger A, *et al.*, 2022, Biomechanical finite element analysis of short-implant-supported, 3-unit, fixed CAD/CAM prostheses in the posterior mandible. *Int J Implant Dent*, 8(1):8.

https://doi.org/10.1186/s40729-022-00404-8

22. Liu B, Li X, Qiu W, *et al.*, 2022, Mechanical distribution and new bone regeneration after implanting 3D printed prostheses for repairing metaphyseal bone defects: A finite element analysis and prospective clinical study. *Front Bioeng Biotechnol*, 10:921545.

https://doi.org/10.3389/fbioe.2022.921545

23. Lemos CAA, Verri FR, Santiago Junior JF, *et al.*, 2018, Splinted and nonsplinted crowns with different implant lengths in the posterior maxilla by three-dimensional finite element analysis. *J Healthc Eng*, 2018:1–7.

https://doi.org/10.1155/2018/3163096

24. Silva LS, Verri FR, Lemos CAA, *et al.*, 2021, Biomechanical effect of an occlusal device for patients with an implant-supported fixed dental prosthesis under parafunctional loading: A 3D finite element analysis. *J Prosthet Dent*, 126(2):223.e1–223.e8.

https://doi.org/10.1016/j.prosdent.2021.04.024

25. Mikushev VM, Samarkin AI, Khomutova AS, 2021, Finite element simulations of stresses in bone implants made by three-dimensional printing. *IOP Conf Series: Mater Sci Eng*, 1117(1):12006.

https://doi.org/10.1088/1757-899X/1117/1/012006

26. Mirulla AI, Di Paolo S, Di Simone F, *et al.*, 2020, Biomechanical analysis of two types of osseointegrated transfemoral prosthesis. *Appl Sci Basel*, 10(22):8263.

https://doi.org/10.3390/app10228263

27. Uğur L, Ozturk B, Erzincanli F, 2022, Reduction of stress variations on sections (ROSVOS) for a femoral component. *Iran J Sci Technol Transact Mech Eng*, 46(1):237–252.

https://doi.org/10.1007/s40997-020-00418-w

28. Öztürk B, Erzincanli F, 2019, Development of femoral component design geometry by using DMROVAS (design method requiring optimum volume and safety). *Eng Comput*, 37(2): 682–704.

https://doi.org/10.1108/EC-03-2019-0077

29. Francisco AV, Raquel CO, Luis-Guillermo OL, *et al.*, 2019, Influence of bone quality on the mechanical interaction between implant and bone: A finite element analysis. *J Dent*, 88:103161.

https://doi.org/10.1016/j.jdent.2019.06.008

30. Cheong VS, Mumith A, Coathup M, *et al.*, 2020, Bone remodeling in additive manufactured porous implants changes the stress distribution, in *Health Monitoring of Structural and Biological Systems XIV; International Society for Optics and Photonics*, *Bellingham, WA, USA*.

https://doi.org/10.1117/12.2558093

31. Zysset PK, Guo XE, Hoffler CE, *et al.*, 1999, Elastic modulus and hardness of cortical and trabecular bone lamellae measured by nanoindentation in the human femur. *J Biomech*, 32(10):1005–1012.

https://doi.org/10.1016/S0021-9290(99)00111-6

32. Rho JY, Ashman RB, Turner CH, 1993, Young's modulus of trabecular and cortical bone material: ultrasonic and microtensile measurements. *J Biomech*, 26(2):111–119.

https://doi.org/10.1016/0021-9290(93)90042-D

33. Arabnejad S, Burnett JR, Pura JA, *et al.*, 2016, High-strength porous biomaterials for bone replacement: a strategy to assess the interplay between cell morphology, mechanical properties, bone ingrowth and manufacturing constraints. *Acta Biomater*, 30(2016):345–356.

https://doi.org/10.1016/j.actbio.2015.10.048

34. Mckown S, Shen Y, Brookes WK, *et al.*, 2008, The quasi-static and blast loading response of lattice structures. *Int J Impact Eng*, 35(8):795–810.

https://doi.org/10.1016/j.ijimpeng.2007.10.005

35. Yan C, Liang H, Raymont D, *et al.*, 2012, Evaluations of cellular lattice structures manufactured using selective laser melting. *Int J Mach Tools Manuf*, 62(2012):32–38.

https://doi.org/10.1016/j.ijmachtools.2012.06.002

36. Bayraktar HH, Morgan EF, Niebur GL, *et al.*, 2004, Comparison of the elastic and yield properties of human femoral trabecular and cortical bone tissue. *J Biomech*, 37(1):27–35.

https://doi.org/10.1016/S0021-9290(03)00257-4

37. Levine BR, Sporer S, Poggie RA, *et al.*, 2006, Experimental and clinical performance of porous tantalum in orthopedic surgery. *Biomaterials*, 27(27):4671–4681.

https://doi.org/10.1016/j.biomaterials.2006.04.041

38. Kowalczyk P, 2006, Orthotropic properties of cancellous bone modelled as parameterized cellular material. *Comput Methods Biomech Biomed Eng*, 9(3):135–147.

https://doi.org/10.1080/10255840600751473

39. Liu L, Shi Q, Chen Q, *et al.*, 2019, Mathematical modeling of bone in-growth into undegradable porous periodic scaffolds under mechanical stimulus. *J Tissue Eng*, 10:1–13.

https://doi.org/10.1177/2041731419827167

40. Palomares KTS, Gleason RE, Mason ZD, *et al.*, 2009, Mechanical stimulation alters tissue differentiation and molecular expression during bone healing. *J Orthop Res*, 27(9):1123–1132.

https://doi.org/10.1002/jor.20863

41. Liu L, Duan J, Shi Q, *et al.*, 2020, Mechanical effect on the evolution of bone formation during bone ingrowth into a 3D-printed Ti-alloy scaffold. *Mater Lett*, 273(2020): 127921.

https://doi.org/10.1016/j.matlet.2020.127921

42. Carter DR, 1987, Mechanical loading history and skeletal biology. *J Biomech*, 20(11–12):1095–1109.

https://doi.org/10.1016/0021-9290(87)90027-3

43. Betts DC, Müller R, 2014, Mechanical regulation of bone regeneration: Theories, models, and experiments. *Front Endocrinol*, 5:211.

https://doi.org/10.3389/fendo.2014.00211